



Investigating the impact of air distribution on spray dryer operability using CFD simulations and pilot-scale experiments

Anneloes P. van Boven^{a,b}, Arend Dubbelboer^c, Tom J.A. Janssen^c, Jewe Schröder^c, Jos J.W. Sewalt^a, Reinhard Kohlus^b, Maarten A.I. Schutyser^{a,*}

^a Food Process Engineering, Wageningen University & Research, P.O. Box 17, 6700 AA Wageningen, the Netherlands

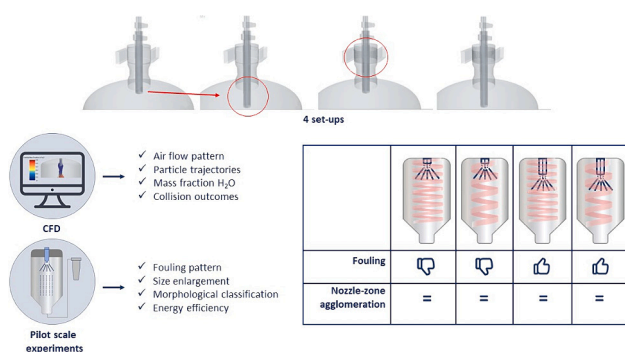
^b University of Hohenheim, Institute of Food Science and Biotechnology, Department of Process Engineering and Food Powders, Garbenstraße 25, 70599 Stuttgart, Germany

^c Danone Nutricia Research, Uppsalaalaan 12, 3584 CT Utrecht, the Netherlands

HIGHLIGHTS

- The nozzle position greatly impacts the fouling of a spray dryer.
- A nozzle position close to the hot air inlet causes more fouling.
- Air distribution seems to hardly affect agglomeration in a single stage dryer.
- Upward air flow can explain fouling by conveying wet particles to the dryer's roof.

GRAPHICAL ABSTRACT



ARTICLE INFO

Keywords:

Spray drying
Fouling
Air distribution
Computational fluid dynamics
Air flow pattern
Agglomeration

ABSTRACT

Fouling reduces spray dryer operability. The impact of different configurations of a spray dryer on operability and nozzle-zone agglomeration stimulated by dry powder dosing was investigated through a combination of CFD simulations and pilot-scale experiments. Included were two positions of the nozzle and dry powder introduction, and two degrees of air swirl. Air flows and droplet trajectories were simulated and a particle collision model was built in. The experiments were executed using a single stage co-current spray dryer with concentric fines return. A high nozzle position (6 cm below the air inlet) resulted in undesired fouling due to an upward air flow causing wet droplets to collide with the roof. The operability was improved by lowering the nozzle position 25 cm as there was less fouling. With a low nozzle position, the degree of air swirl only had a limited effect on fouling. Surprisingly, agglomeration did not seem to be significantly affected by air distribution in both the simulations and the experiments. This means that there is some freedom in the design of a spray dryer in terms of agglomeration. Overall, the findings highlight the importance of well-designed spray drying operations to reduce fouling and thus minimize product waste.

* Corresponding author.

E-mail address: maarten.schutyser@wur.nl (M.A.I. Schutyser).

<https://doi.org/10.1016/j.powtec.2024.119779>

Received 1 March 2024; Received in revised form 29 March 2024; Accepted 15 April 2024

Available online 19 April 2024

0032-5910/© 2024 The Author(s). Published by Elsevier B.V. This is an open access article under the CC BY license (<http://creativecommons.org/licenses/by/4.0/>).

1. Introduction

Spray drying is a commonly used drying method in a wide range of industries, including the food, pharma, chemical, and detergent industry. Spray dried powders have extended shelf life and are appreciated for their excellent techno-functional properties thanks to the possibility of steering the degree of agglomeration of powder during the spray drying process. However, spray drying is also a very energy-intensive process and it is crucial that spray drying conditions are optimized to minimize energy use while having good operability. A spray dryer has good operability when the product quality is well-controlled and there is a high yield and thus minimal fouling. Fouling is undesired because running time is shortened due to the necessity of cleaning and valuable product is lost by sticking to the wall. Besides the economic impact of fouling, minimal fouling is also important for product quality and process safety. Wall deposits can be thermally damaged by the longer exposure to heat which can affect final product quality and safety when falling off and mixing with the product. Moreover, the location of the fouling is important. Deposits in or near the air inlet (region with the highest temperature) introduce a process safety risk in case they start to smolder which can result in a fire or an explosion [1].

Fouling in spray dryers can occur due to sticking of droplets colliding with the walls of the dryer [2]. Spray dryer optimization in practice often relies on the so-called stickypoint which is about 10–30 °C above the glass transition temperature [3]. When particles are not sufficiently dried, this will lead to fouling. In addition to material properties, especially the internal air flow pattern in the spray drying chamber is of importance since an ill-designed air distributor in combination with chamber design can lead to dramatically enhanced fouling [4]. Contact between wet droplets or still sticky powder particles and the wall must

thus be prevented.

Each type of spray dryer comes with its own air distributor design, adapted to the drying chamber and the desired air flow pattern. The air distributor plays a pivotal role in determining the powder quality and operability of the spray dryer. A well-designed air distributor facilitates 1) optimal use of the entire drying chamber volume for drying, 2) good dispersion of droplets and particles in the chamber without undesired particle recirculation into the hot air zone, and 3) good distribution of air to enhance drying and avoid fouling of the wall by undried particles [4]. Different air distributor types are used in industrial spray dryers. Two types of air flow patterns are common for co-current single-stage spray dryers mostly used in the food industry. The first type provides a swirling air flow varying in degree of swirl and the second type provides a direct downward airflow (Fig. 1). A swirling air flow is commonly used in combination with rotary atomizers, while a downward airflow is usually combined with a pressure nozzle or two-fluid nozzle. However, even for the same air flow pattern, suppliers have their own specific air distributor design. The air distributor in combination with the drying chamber dimensions (wide versus tall) determines the full air flow pattern and thus also drying droplet trajectories in the drying chamber [5].

Besides wall deposition leading to fouling, the drying droplet trajectories also influence the collision probabilities between droplets. Colliding droplets can stick together to form agglomerates. This is beneficial, as small particles (<100 μm) negatively affect the functional properties of a powder and are therefore undesired. Often agglomeration is further enhanced by introducing fine dry particles (“fines”) at the top of the chamber [6]. In dryers with such fines return, fines are recirculated until sufficiently big. The success of agglomeration does not only depend on the collision probability but also on the sticking probability: depending on the droplet’s properties at the moment of collision,

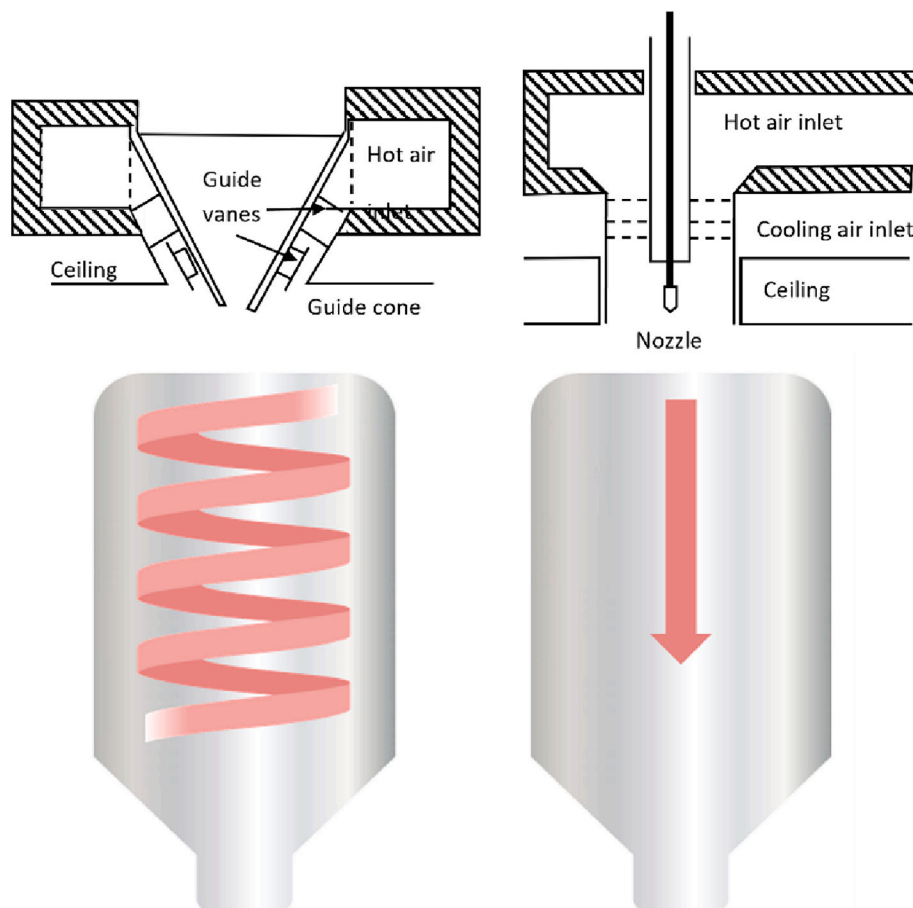


Fig. 1. Air dispersers (top) and resulting air flow pattern (bottom) for rotary air swirl (left) and straight downward flow (right). Schematic air distributor drawings are adopted from Pisecky (2012) [31].

they will either coalesce, agglomerate, or bounce [7]. The stickiness can be altered by adapting the drying conditions [3,8], but also by the exact position at which the fine dry particles are (re)introduced in the drying chamber [6]. This position also affects the collision probability, as the dispersion of droplets and particles increases with increasing distance from their respective introduction position, lowering the probability of a collision. Achieving proper agglomeration on an industrial scale is usually a trial-and-error process for every different dryer and product. This leads to products that need to be reworked or discarded, contributing to undesirable energy use and material loss.

Hitherto, unfortunately, limited experimental studies have been conducted on the influence of air distributor design on air flow patterns and resulting agglomeration, as usually, the air distributor design is a given for a spray dryer installation. Several previous studies used computational fluid dynamics (CFD) to predict air flow patterns and particle histories, including temperature, velocity, and residence time in spray dryers [9]. For example, Ruprecht & Kohlus (2019) compared a swirl air distribution to a parallel one by modeling the residence time distributions of particles using CFD. The residence time distributions of the centrifugal air disperser had more variation, indicating a less stable flow pattern [10]. The particle residence time using the centrifugal air distributor was longer than that of the parallel one [11]. Several researchers have also used CFD to predict fouling in spray dryers based on particle stickiness [12–14]. Others used stickiness predictions to predict zones in spray dryers where coalescence and agglomeration could take place [3,15]. Other researchers even modeled the phenomenon of agglomeration during spray drying aiming at the prediction of powder agglomerate size [16,17]. CFD studies did not cover the effect of air distribution on agglomeration. The reason for this is that agglomeration is much more difficult to model than only air flow distribution. Hence, experimental studies are needed to link air flow patterns and agglomeration outcomes.

Therefore, with this research, we aim to understand the effect of air flow pattern on the operability of a spray dryer by combining CFD simulations with experiments. Pilot trials with a single stage, co-current spray dryer in different configurations were executed while dosing powder particles (fines) concentrically to the nozzle. Two degrees of air swirl are compared, and the position of the nozzle and fines dosing place is varied from the top of the drying chamber to a lower position. Fouling is assessed visually by comparing fouling patterns and by comparing the yield. Furthermore, the extent of agglomeration in the produced powder was assessed by scanning electron microscopy, particle size distribution analysis, and classifying individual particles as primary particles, partially coalesced particles, or agglomerates using image-based morphology analysis. CFD simulations were used to explain the findings by investigating if and where atomized droplets collide with the fines in the drying chamber, and the resulting collision outcomes. For this, we have built in a collision model based on previous work from Finotello et al. [18]. The novelty of our study lies in exploring the effect of different air distributor configurations in spray dryers, a topic rarely investigated due to the usual fixed designs. We combine CFD simulations with pilot-scale experiments to reveal how air flow patterns affect the operability of a spray dryer. The results give new insights into how air distribution affects operability and agglomeration in a spray dryer. Spray dryer equipment manufacturers can use these insights to design better air distributors.

2. Materials and methods

2.1. Materials

Maltodextrin DE21 (MD21) (Glucidex 21, Roquette Frères, France) was used as model material. Ponceau red E124 (Natural Spices, the Netherlands) was used as colorant. Regular hot tap water (50 °C) was used to prepare the feed.

2.2. Spray dryer configurations

The experimental trials were conducted using a DW-350 single-stage pilot scale spray dryer from Spray Dry Works (the Netherlands) (Fig. 2), which was also the subject of the CFD simulations. The drying chamber is 2 m tall and 1.5 m in diameter. Four different configurations were used (Fig. 3). Set-up A, referred to as original, has a strong air swirl and the nozzle and fines introduction are located at the top of the drying chamber. Set-up B, referred to as basket, has a reduced air swirl by placing a perforated basket in the air disperser. Set-up C, referred to as extension, has a strong air swirl, but the nozzle and fines introduction is positioned 25 cm lower in the drying chamber by extending the pipes through which they are introduced. Set-up D combines the perforated basket for a reduced air swirl and the lower placement of the nozzle and fines introduction. A detailed picture of the perforated basket can be found in Appendix 1, Fig. A1.

2.3. Trials with fines dosing

For all spray drying trials, a 40% w/w MD21 feed was prepared by dissolving the powder in hot tap water and stirring for at least 30 min until the solution became transparent. Each time a feed rate of 25 kg·h⁻¹ was applied to a SIY78/SKY16 high pressure nozzle from Spraying Systems Co. (USA), resulting in an atomization pressure of 56.5 ± 2.9 bar. The feed temperature at atomization varied between 30 and 34 °C.

A Condaire DA 1400 desiccant dryer (Switzerland) was used to dehumidify ambient air to a relative humidity of 5%. Subsequently, an electrical heater heated the air to the inlet temperature of 180 °C. The drying air flowrate (dry basis) was 540 kg·h⁻¹. The powder was separated from the drying air using a cyclone and subsequently collected via a rotary valve. Because the atomization condition was kept constant, the outlet temperature was not set to a specific value.

Agglomeration was stimulated by dosing dry, small powder particles, so-called “fines”, concentrically to the nozzle. These fines are produced separately (see 2.3.1) and added to the process; they are not originating from inline-separation of the fine fraction from the produced powder. They were dosed using a screw at a mass flow rate of 15.9 kg·h⁻¹ and transported using ambient air by a small fan. For every set-up, a setting with and without fines dosing was included.

After the trials, pictures were taken of the drying chamber and the nozzle to be able to compare the fouling pattern and operability of the different configurations.

The energy efficiency (η) of the trials was calculated using Eq. (1)

$$\eta = \frac{\dot{Q}_{\text{required}}}{\dot{Q}_{\text{in}}} \cdot 100\% = \frac{(X_f - X_p) \cdot \dot{m}_f \cdot \Delta h_v}{\dot{Q}_{\text{feed}} + \dot{Q}_{\text{dry air}}} \cdot 100\% \text{ with}$$

$$\dot{Q}_{\text{feed}} = \dot{m}_f \cdot h_f = \dot{m}_f \cdot ((c_{p,s} + X_F \cdot c_{p,w}) \cdot (T_f - T_{\text{ref}}))$$

$$\dot{Q}_{\text{dry air}} = \dot{m}_{\text{da}} \cdot h_{\text{da}} = \dot{m}_{\text{da}} \cdot ((c_{p,a} + AH_{\text{da}} \cdot c_{p,wv}) \cdot (T_{\text{da}} - T_{\text{ref}}) + AH_{\text{da}} \cdot \Delta h_v) \quad (1)$$

in which $\dot{Q}_{\text{required}}$, \dot{Q}_{in} , \dot{Q}_{feed} and $\dot{Q}_{\text{dry air}}$ are the amount of heat per unit time required, going in provided by the feed and provided by the dry air respectively [kJ·h⁻¹]. X_f and X_p are the mass fractions of water in the feed and the product (dry basis) [kg water · kg dry mass⁻¹], \dot{m}_f the mass flow rate of the feed (dry basis) [kg·h⁻¹], Δh_v the latent heat of vaporization [kJ·(kg·K)⁻¹], h_f and h_{da} the specific enthalpy supplied by the feed and dry air [kJ·kg⁻¹], $c_{p,s}$, $c_{p,w}$, $c_{p,a}$ and $c_{p,wv}$ the specific heat capacities of the solute, water, air, and water vapor [kJ·(kg·K)⁻¹], and AH_{da} the absolute humidity of the dry air [kg·kg⁻¹].

2.3.1. Fines production

Fines were produced following the method from van Boven et al. (2023) [8]. A feed with a total solids content of 40% w/w (99.625 wt% MD21 and 0.375 wt% ponceau red) was atomized using a SU2A two-

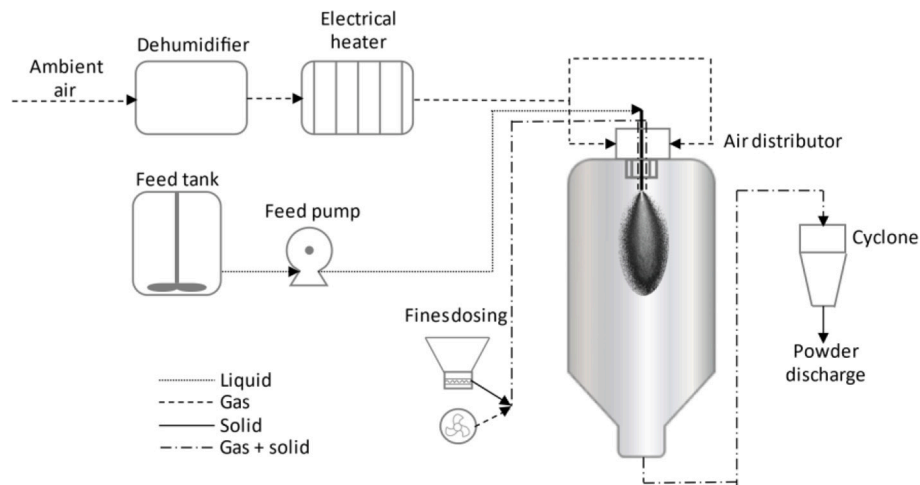


Fig. 2. Schematic overview of the DW-350 pilot-scale spray dryer, not to scale.

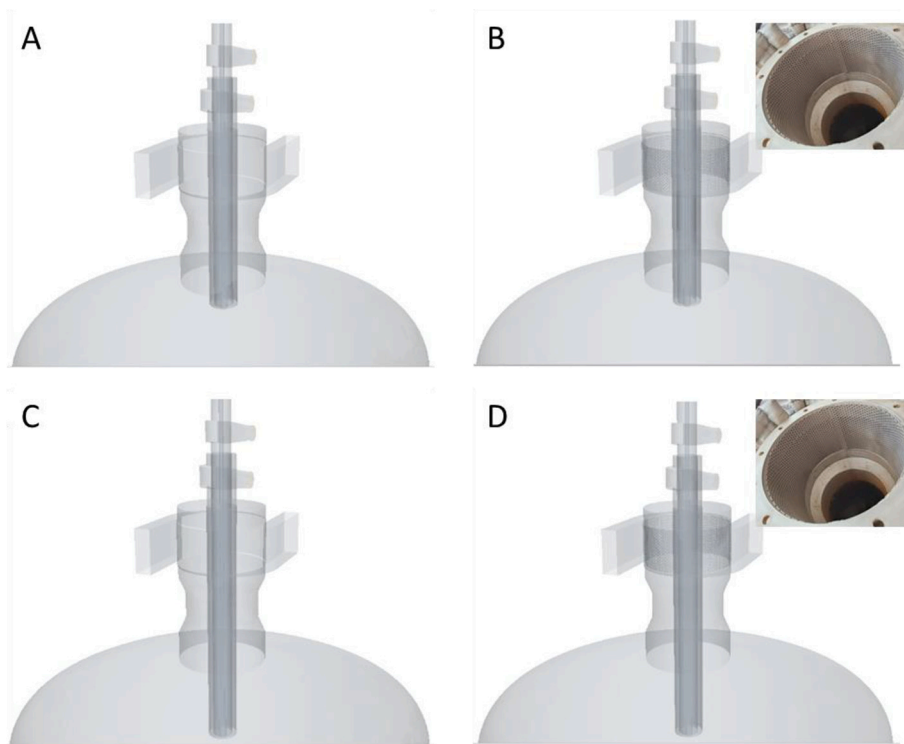


Fig. 3. Different configurations of the pilot scale spray dryer. A: original, B: basket, C: extension, D: basket & extension. A picture of the perforated basket is added to the configurations that use it.

fluid nozzle (Fluid Cap 2050, Air Cap 70) (Spraying Systems Co., USA) with an atomizing pressure of 414 kPa. The collected powder was air classified using a Hosokawa Alpine Multi-mill system with an integrated air classifier (rotor speed 5000 rpm, inlet air flowrate of 40–55 m³h⁻¹, pressure drop across the classifier 1.2–3.3 kPa) to obtain a fraction with a small particle size. This fraction had a D(4,3) of 20.8 ± 0.4 μm.

2.4. Powder analysis

2.4.1. Powder morphology

The powder samples were visually compared using scanning electron microscopy (SEM). For SEM analysis, the powder was adhered to the aluminum sample holder using carbon tape. Any loose particles were removed by blowing with pressurized air. The samples were gold coated using a JEOL Smart-Coater (JEOL, Japan). Images were then taken using

a JCM-7000 SEM (JEOL, Japan) at an acceleration voltage of 5 kV.

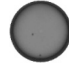


Additionally, particles were classified according to their morphology using a Malvern Morphologi 4 (Malvern, UK). Per sample, 19 mm³ of powder was dispersed onto a glass plate (dispersion pressure 2.5 bar) and image analysis was used to obtain their descriptive shape factors. The classification was done according to van Boven et al. (2023), Table 1. A further division was made into three size classes based on the circle equivalent (CE) diameter: <15 μm, 15 ≤ x < 30 μm and ≥ 30 μm. The powders were analyzed in duplicate. For each measurement, between 24,000 and 40,000 particles were analyzed.

2.4.2. Particle size

The particle size distribution (PSD) of the powders was determined using a Mastersizer 3000 equipped with an Aero S dry dispersion unit (Malvern Panalytical, UK). The standard Venturi dispenser was used

Table 1

Particle classes based on shape factors obtained from the Malvern Morphologi 4 software. Particles that did not belong to any of these classes were classified as ‘other’ (N_o) [8].

Particle class	High Sensitivity (HS) circularity	Elongation	Solidity ($\frac{\text{actual area}}{\text{convex hull area}}$)	Example particle and corresponding CE-diameter
Primary particles (N_{pp})	≥ 0.98	< 0.1	> 0.6	 52.3 μm
Partially coalesced particles (N_{pc})	$0.98 > \dots \geq 0.8$	< 0.7	> 0.6	 54.6 μm
Agglomerated particles (N_{agg})	< 0.8	< 0.7	> 0.6	 75.8 μm

with a dispersion pressure of 1.0 bar. The data was analyzed with the Mie theory for non-spherical particles with a refractive index of 1.68 and an absorption parameter of 0.01 as optical properties.

The change in particle size induced by fines dosing was visualized using a difference plot. This was done according to the method of Williams et al. [19], as also used by van Boven et al. [8]. First, the mass fraction of atomized MD21 particles in the final powder ($x_{\text{atomized MD21}}$ in $\text{kg}\cdot\text{kg}^{-1}$) was calculated using Eq. (2):

$$x_{\text{atomized MD21}} = \frac{TS_{\text{feed}} \cdot \dot{m}_{\text{feed}}}{TS_{\text{feed}} \cdot \dot{m}_{\text{feed}} + \dot{m}_{\text{fines}} \cdot (100 - MC_{\text{fines}})} \quad (2)$$

where TS_{feed} ($\text{kg}\cdot\text{kg}^{-1}$) is the total solids content of the feed, \dot{m}_{feed} ($\text{kg}\cdot\text{h}^{-1}$) is the mass flowrate of the feed, and MC_{fines} is the moisture content of the fines determined by oven drying in duplicate. Then, a theoretical PSD of the sample was calculated by mixing the PSDs of the unagglomerated sample (no fines dosing) and of the fines in their corresponding mass fractions using Eq. (3).

$$\text{PSD}_{\text{theoretical}} = x_{\text{atomized MD21}} \cdot \text{PSD}_{\text{unagglomerated}} + (1 - x_{\text{atomized MD21}}) \cdot \text{PSD}_{\text{fines}} \quad (3)$$

A difference curve was then created by subtracting the $\text{PSD}_{\text{theoretical}}$ from the sample PSD (Eq. (4)).

$$\Delta\text{PSD} = \text{PSD}_{\text{sample}} - \text{PSD}_{\text{theoretical}} \quad (4)$$

In this difference curve, the negative areas represent the particle sizes that have disappeared and the positive areas represent the particle sizes that appeared due to agglomeration.

2.5. CFD

The CFD model was built in STAR-CCM+ (V2022.1) [20]. Here a general model set-up will be described, for the model details the reader is referred to the manual of STAR-CCM+. Specific model choices are described below. The physical model parameters, mesh parameters, and solver parameters are summarized in Appendix 2.

2.5.1. Air streams in a spray dryer

Three inlet air streams were modeled: the main air stream used for evaporation, the shielding cooling air stream needed for protection of the nozzle and lance, and the fines transportation air. There is one outlet air stream at the bottom of the spray dryer.

All air streams were treated as Eulerian phases and were modeled as ideal gasses. The turbulence is modeled with the Elliptic Blending k - ϵ model. The Elliptic Blending turbulence model solves transport equations for the turbulent kinetic energy, the turbulent dissipation rate, the normalized (reduced) wall-normal stress component, and the Elliptic Blending factor to determine the turbulent eddy viscosity [21].

2.5.2. Maltodextrin particles model

2.5.2.1. Lagrangian particles model. The maltodextrin particles were treated as Lagrangian particles. Two-way coupling is activated as well as turbulent dispersion, drag, the TAB secondary droplet break-up model, evaporation (see 2.5.2.2), and the pressure gradient force. The pressure gradient force is caused by a gradient in the static pressure of the air. A static pressure gradient was observed near the nozzle. For model details, the reader is referred to the STAR-CCM+ manual (version 2022.1).

The maltodextrin solution was injected into the Eulerian domain with a velocity and droplet size distribution calculated by the Linearized Instability Sheet Atomization (LISA) model [22]. The fines were injected as completely dry particles at the same speed as the fines transportation air. The particle size distribution of the fines (determined experimentally (Section 2.4.2, Appendix 1, Fig. A2) was used as input for the CFD model.

2.5.2.2. Droplet evaporation model. To simulate the moisture content of the maltodextrin droplets throughout the spray dryer, a droplet evaporation model was activated. The quasi-steady droplet evaporation model from STAR-CCM+ assumes droplets to be internally homogeneous. The Ranz-Marshall correlation was used to calculate the Sherwood number. For modeling the drying of maltodextrin droplets turning to particles, the characteristic drying curve approach of Saleh (2010) is employed [23]. To implement the characteristic drying curve the evaporation rate was multiplied by a factor ξ (Eq. (5)) to account for the hindered drying regime.

$$\xi = \left(\frac{x - x_{\text{eq}}}{x_{\text{cr}} - x_{\text{eq}}} \right)^n \quad (5)$$

where n is determined to be equal to 3.22 for maltodextrin, The critical moisture content x_{cr} was assumed equal to the initial water mass fraction (0.6 in this case) as the characteristic drying curve is material dependent and not influenced by external drying conditions [23], and x_{eq} is modeled with the sorption isotherm (6):

$$x_{\text{eq}} = \frac{1}{100} \left[\frac{\ln(1 - \psi)}{-c_1(T + c_2)} \right]^{1/m} \quad (6)$$

where c_1 , c_2 , and m are equal to 0.000405, -187.962 and 1.169 , respectively [23]. Furthermore, T is the air temperature in Kelvin and ψ is the relative humidity as a fraction from 0 to 1. The relative humidity is calculated as the fraction of the actual water vapor fraction (determined from the ideal gas law) over the saturation water vapor pressure (determined from the Antoine equation with $A = 8.07131$, $B = 1730.63$, and $C = 233.426$).

2.5.2.3. Particle collision model. Particle collisions in the transient simulations were simulated using the NTC (No Time Counter) collision model. This model first detects particle collisions and subsequently calculates the collision outcome. The outcome of a collision depends on the collision Weber number, We , and the impact parameter B . In the O'Rourke method, a map is generated where all collision outcomes are a function of the collision Weber number and the collision efficiency E ($E = B \cdot B$) [24].

Droplets bounce off from each other (simple bounce or reflexive separation), coalesce, or graze each other (stretching separation) according to their position on the collision outcome map. The droplet collision experiments of Finotello et al. (2018) [18] are used to shape the collision outcome map. The parameters describing the boundaries of the collision outcome regimes are listed in Appendix 2. To compare the different spray dryer geometries, the particle collision outcomes were monitored in a fixed virtual volume below the nozzle. The volume was a cylinder with a height of 0.5 m and a radius of 0.3 m. All collision outcomes within this cylinder were counted and summed up for comparison.

The collision model requires a transient approach to CFD. A fully resolved air flow field was obtained from the steady simulations. At time $t = 0$ the particles were injected. In the experiment the fans were turned on first and only later the feed was injected.

3. Results and discussion

3.1. Steady state air flow patterns

The steady state air flow patterns obtained from the CFD simulations (Fig. 4) show the effect of the modifications on the air flow. The air flow

patterns of the original air distributor (A and C) seem less chaotic compared to when the perforated basket is inserted (B and D). Inserting a basket in the air distributor reduces the radial velocity of the air flow (Fig. 5, Appendix 1 Fig. A3). Without the basket, the high air velocity creates a strong swirling air flow which generates lower pressures around the center pipes, resulting in an upward flow of the air close to the central pipe. This is depicted by the streamlines turning around at the end of the pipe and not continuing further into the chamber (Fig. 5, A&C). Inserting the perforated basket reduces the air swirl and hence the upward flow. When combining the perforated basket with the extension (D), the air flow does not show any upward motion next to the central pipe.

In all simulations, vortices appear in the spray dryer. They mainly depend on the air inlet design. A stratified inlet air flow (e.g. [25]) shows different behaviour from a swirling inlet air flow as described in this paper.

3.2. Particle trajectories

Due to long computation times, all simulations were run for 0.215 s after initiating the feed and fines injection. The shape of the spray cone and fines trajectories within the drying chamber were influenced by the different configurations and their corresponding air flows (Fig. 6). The upward air flow in the original configuration (A) carries both wet and dry particles. With the extension (C), the upward air flow only takes the dry particles to the top of the drying chamber. The basket configuration (B) exhibited the most chaotic air flow pattern (Fig. 4B). The air seems to take the dry particles upwards (Fig. 6B). It can also be seen that a fraction of these is directed sideways to the wall of the drying chamber. In configuration D the spray and the fines seem to go most stable in a

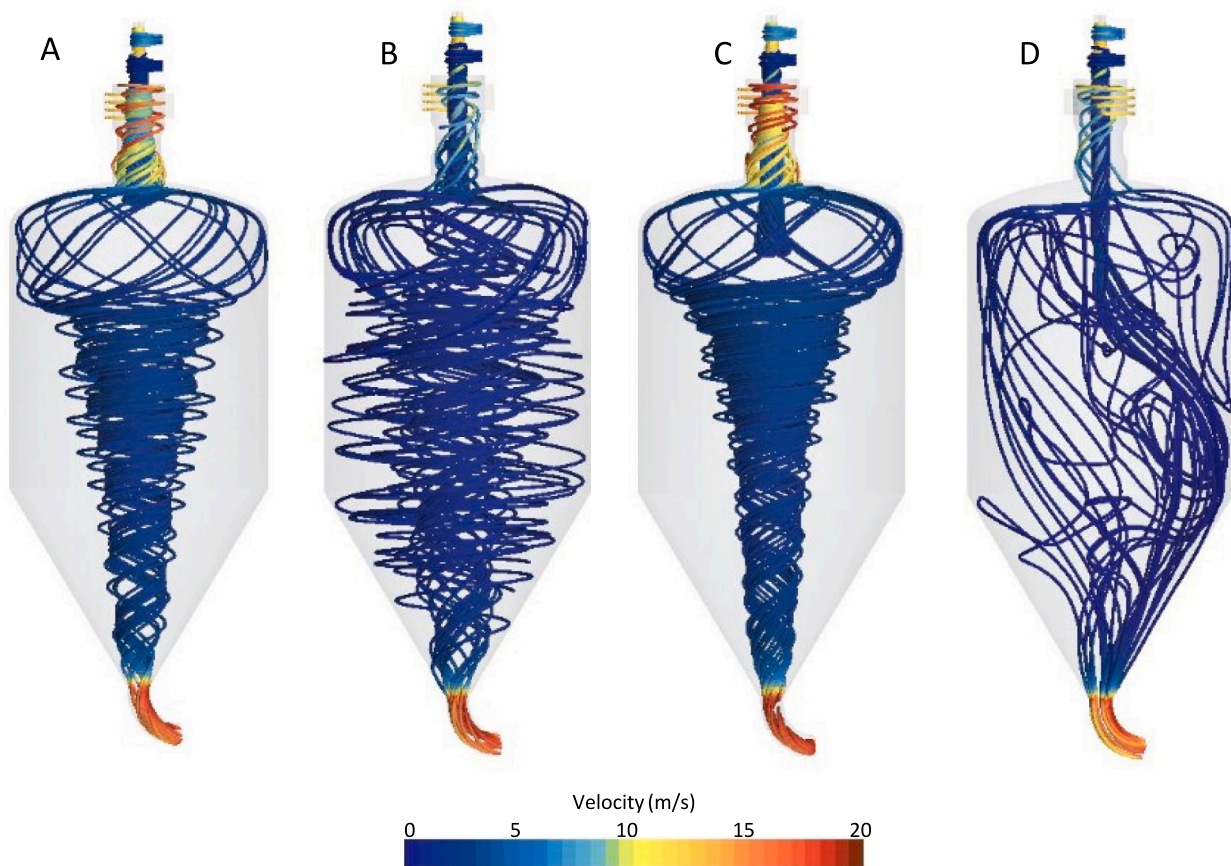


Fig. 4. Steady state air velocities in the different configurations. For clarity, only streamlines from one arm of the air distributor are used, but air flows through both. Configurations are A: original, B: basket, C: extension, D: basket & extension.

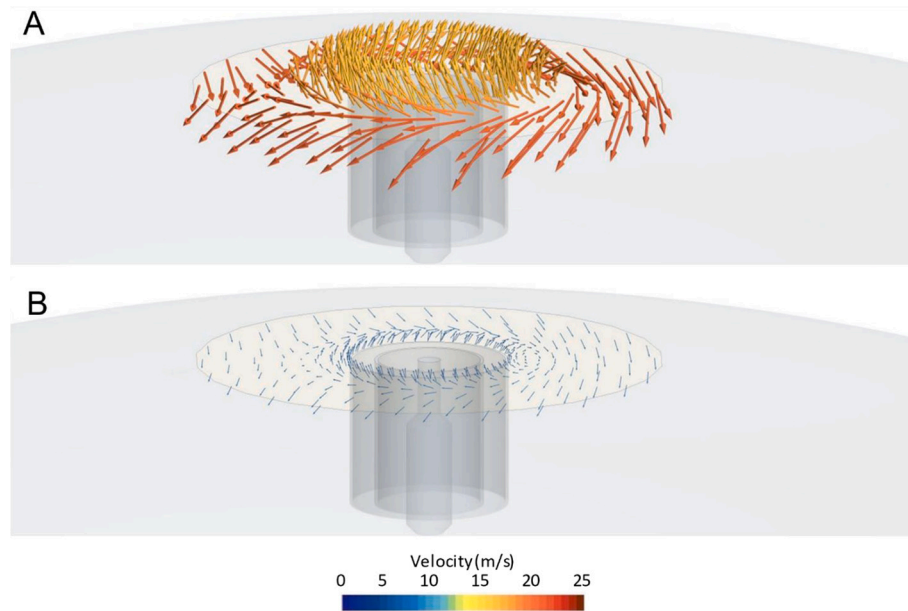


Fig. 5. Effect of the perforated basket on air flow velocity vectors. A: original, B: basket.

downward direction, which matches the steady state air flow pattern that was also most stable for this configuration. Although there is no upward flow visible around the center pipe, there still is an upward air flow in the rest of the chamber visible (Fig. 4D). This flow may take droplets upwards and eventually, they may reach the roof or internal tubes of the dryer and deposit there.

3.3. Operability

The different configurations of the pilot-scale spray dryer led to different visually observed fouling patterns in the drying chamber (Fig. 7). In the original configuration (A), the fouling occurred mainly on the roof of the drying chamber and on the tubes through which the nozzle and fines enter the drying chamber. The CFD simulations indicate a strong upward flow of both wet and dry particles. Although not simulated, the result is that in practice these particles collided with the roof and caused fouling there. Fouling at the roof or on the tubes is undesired because this is also the place where the hot air is introduced.

The presence of burnt powder particles (or scorch) negatively affects powder quality. Moreover, it increases the risk of smoldering when deposits form in hot areas of a spray dryer. In the basket configuration (B), more fouling occurred in the lower part of the drying chamber. This is also reflected in the yield (Table 2). The ceiling of the drying chamber remained clean, but there was more fouling at the tubes through which the lance with the nozzle and the fines were introduced. There was even fouling on the nozzle itself, which is also referred to as bearding. Over time, this build-up can prevent proper atomization of the feed and requires cleaning. The bearding also increases the safety risk of smoldering. This configuration is therefore inoperable. Fig. 6B shows mainly dry particles that are brought upwards, which does not explain this bearding. However, the air flow in this configuration is relatively chaotic (Fig. 4B). It is possible that the atomized droplets are brought up by the air after the 0.215 s from the simulation, and then end on the tubes. The extension configuration (C) resulted in a clean top of the drying chamber, no bearding, and limited fouling in the lower part of the drying chamber and is thus well-operable. In the CFD simulations, an

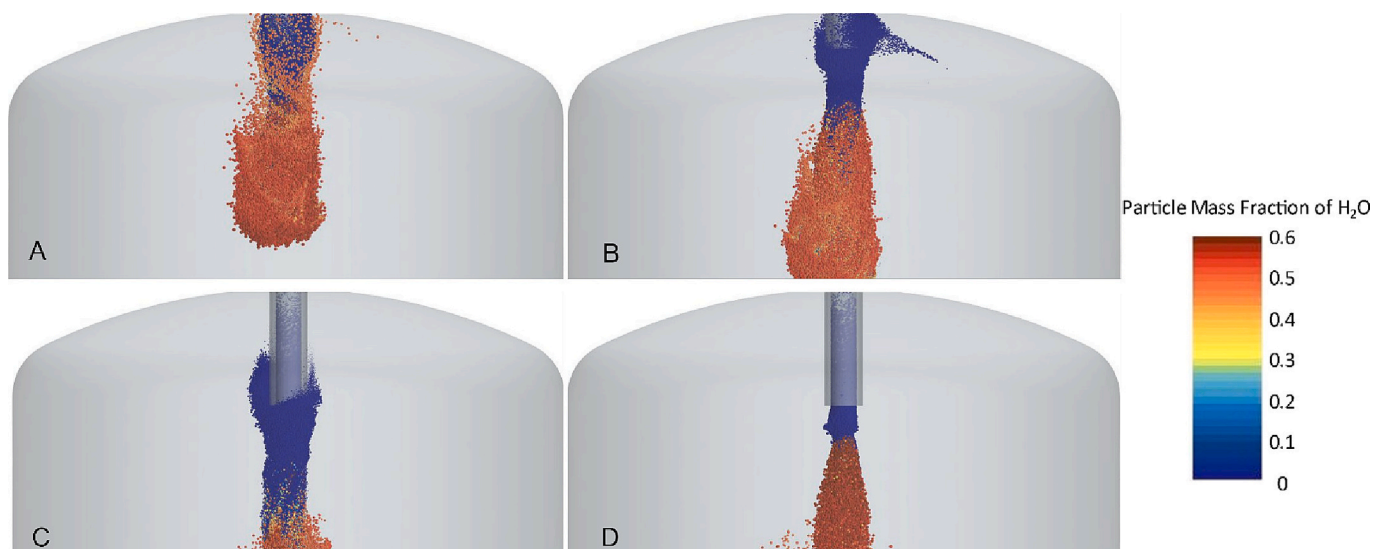


Fig. 6. Particles and their moisture content in the drying chamber 0.215 s after injection. A: Original, B: basket, C: extension, D: basket & extension.

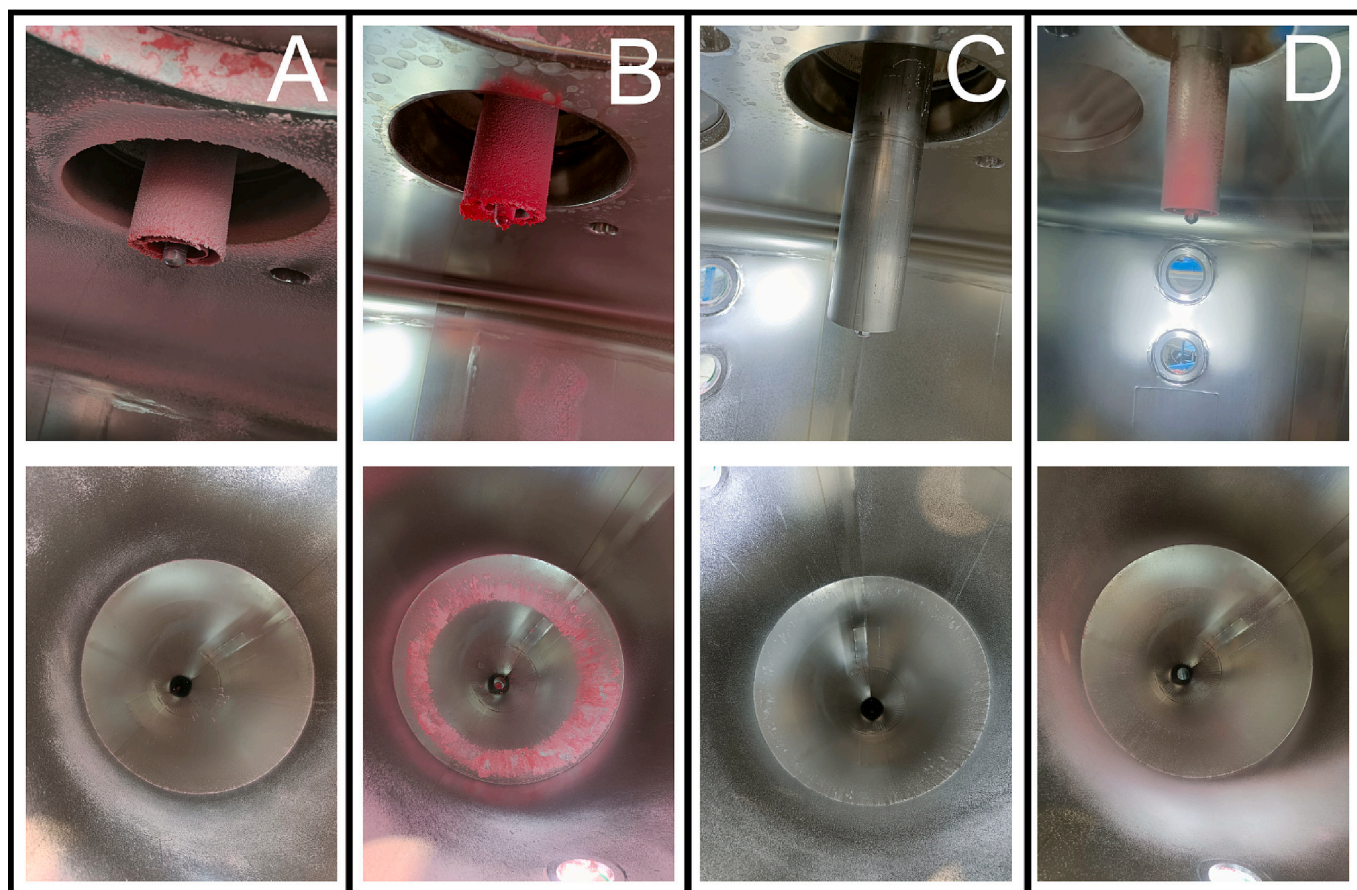


Fig. 7. Pictures of the fouling in the drying chamber after the trials. The top row is a picture of the nozzle zone, bottom row is taken at the top of the drying chamber looking down. A: Original, B: basket, C: extension, D: basket & extension.

Table 2

Process settings of experimental trials. For every set-up, a sample with and without fines dosing was included.

Set-up	T_{out} (°C)	Dry air flow (kg/h)	Fines flow (kg/h)	Energy efficiency (%)	MC (%)	Yield (%)
A: Original	84	537	–	29.0	2.5	90.1
	83	547	15.9	29.3	2.2	75.4
B: Basket	93	548	–	29.3	2.2	91.2
	93	513	15.9	31.4	2.1	65.6
C: Extension	82	550	–	29.3	1.5	84.9
	81	548	15.9	29.4	1.5	69.7
D: Basket & extension	86	541	–	29.5	3.4	89.4
	85	548	15.9	28.8	3.4	71.1

upward flow was visible, but this consisted primarily of dry particles. These particles do not stick, thus indicating a clean roof of the drying chamber in practice. The configuration that combines the basket and the extension (D) resulted in some powder on the bottom part of the nozzle and fines tubes, but no bearding. The lower part of the drying chamber showed an asymmetrical particle deposition pattern. Overall, the fouling in this configuration is considered limited, and this configuration is thus also well-operable. The CFD simulations showed the most stable downward flow, with a small upward flow of droplets on one side (Fig. 6D, left). Although these droplets did not reach the extended tubes within the simulation time, it is expected that they will reach that point upon extending the simulation time. This is reflected by the fouling on these tubes in the experiments. The asymmetry of the droplets in the CFD pattern is in line with the asymmetrical fouling in the experiments.

Langrish et al. [26] performed a study where they simulated the wall deposition rates in a spray dryer and compared it to experimental results. It was found that a high swirl increased the degree of recirculation

in the drying chamber, but also decreased the wall deposition rate. In our situation, installing the basket (B) (decreasing, but not eliminating the swirl) led to more wall deposition in the conical region of the dryer and less fouling at the top, which matches these findings. However, in the extension configuration (C) there is less fouling visible compared to the original situation, while the level of swirl is the same. This highlights the importance of the location of the spray and fines introduction.

The yield is lower for the samples that used fines dosing compared to those that did not include fines dosing (Table 2). This can be explained because after the drying chamber, the particles are separated from the air in a cyclone, which is more efficient for larger particles. Therefore, a larger fraction of the product is lost when fines are introduced. However, because the feed rate, fines dosing rate, and air flow remained the same, it is assumed that the impact would be the same in all configurations and a comparison was still possible.

The outlet temperature of the trials differed (Table 2). During the trials, it was most important that the atomization would be the same

over all the trials. That is why it was decided to keep the feed flow the same and accept differences in outlet temperature. Changes in surrounding temperature might affect the heat loss. There were some larger deviations for set-up B (basket). Besides the outlet temperature, also the dry air flow differed. The air flow was set as close as possible to 550 kg/h for the no fines condition. Adding the fines changed the density of the air, affecting the dry air flow. In this condition, this effect seemed to be larger. However, the other values such as yield and energy efficiency seemed to be in the same range as the other samples.

Industrial spray dryers typically have energy efficiencies of approximately 65%, or <50% for heat sensitive products [27]. The energy efficiency values of this research (Table 2) may seem low. However, pilot-scale spray dryers usually have lower energy efficiencies, as their surface-to-volume ratio is disadvantageous. The values can also fluctuate a lot depending on the processing conditions. For example, a study using a Niro Production minor (1.78 m tall, 1.20 m diameter) found values varying from 27.6 up to 73.2% for the same product in different drying conditions [28]. For a Büchi spray dryer (lab-scale) low energy efficiencies between 7.5 and 8.5% are reported [29].

3.4. Agglomeration

3.4.1. Visual observations powder

Upon visually comparing the powdered samples (Fig. 8), it is evident that the produced powders contain mainly loose particles, mixed with some small agglomerates. In spray dryers with re-circulation of fines, these can have multiple passes through the nozzle zone [30], so it cannot be expected for the utilized pilot dryer that the final powder consists of agglomerates only. Although visual observations are difficult and only qualitative, it seems that the basket set-up and the basket & extension set-up contain slightly more agglomerates than the other set-ups. The basket & extension set-up also contains some larger agglomerates.

3.4.2. Particle size enlargement

The particle size distributions (Appendix 1, Fig. A2) of the different configurations were similar. Therefore, difference curves were created to compare the particle size enlargement from fines addition in the different configurations (Fig. 9). The basket configuration had the most particle size enlargement, followed by the basket & extension configuration. The original configuration and the extension had similar size enlargement. The difference curves are in line with the visual observations from the SEM images that the basket and basket & extension set-up contain more agglomerates than the other two.

3.4.3. Powder morphology classification

The results of the powder morphology classification (Fig. 10) are within the range of earlier classifications of powders produced with a single pass fines dosing [8]. However, the differences are very small and they are not in line with the results from the particle size difference plot (Fig. 9). Based on the difference plot, the highest fraction of partially coalesced and agglomerated particles was expected for the basket (B) and basket & extension (D) configuration. However, the extension configuration (C) seems to have a slightly (though non-significant) bigger fraction of agglomerates and partially coalesced particles than the basket configuration (together 51.0% and 50.7% respectively of all size classes combined). The basket & extension (D) configuration has a smaller fraction at 45.8%, and thus the largest fraction of primary particles.

A possible explanation for these contradictory results might be that in the basket & extension configuration, the particle size enlargement has been caused by full coalescence. When droplets collide while being in a more wet state, the collision outcomes shift more towards full coalescence. This means that droplets merge completely or completely cover a fine. In the resulting powder particle therefore no individual structures can be identified and the particle is classified as a primary particle. Size enlargement based on full coalescence is limited [7], which

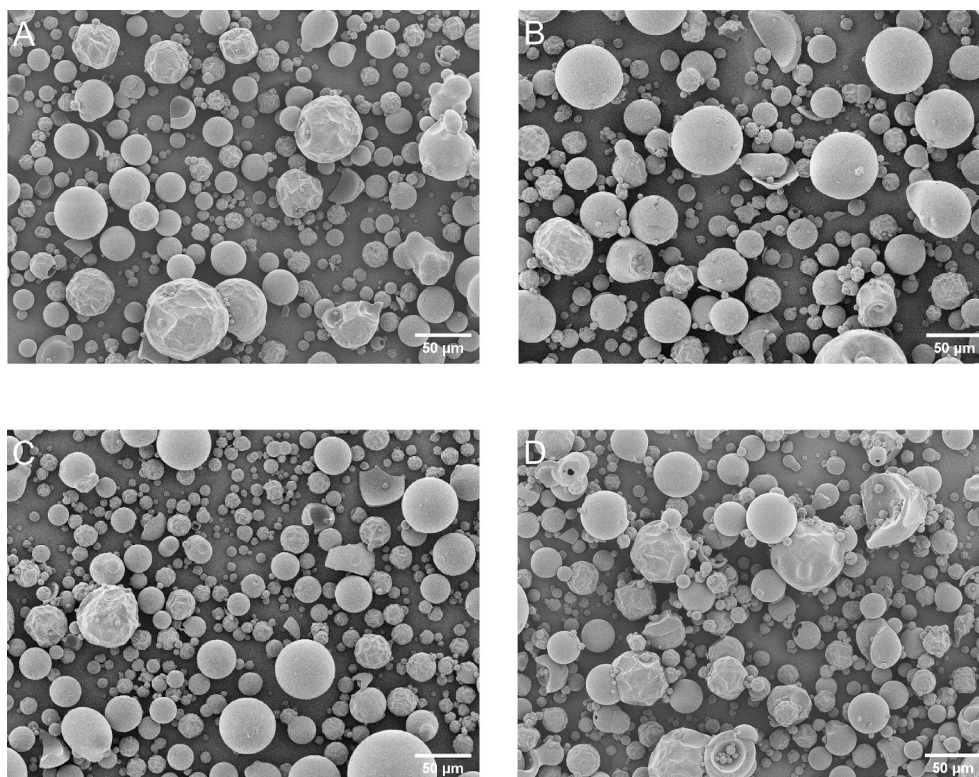


Fig. 8. SEM images of samples from powder trials in the different set-ups: A: original, B: basket, C: extension, D: basket & extension.

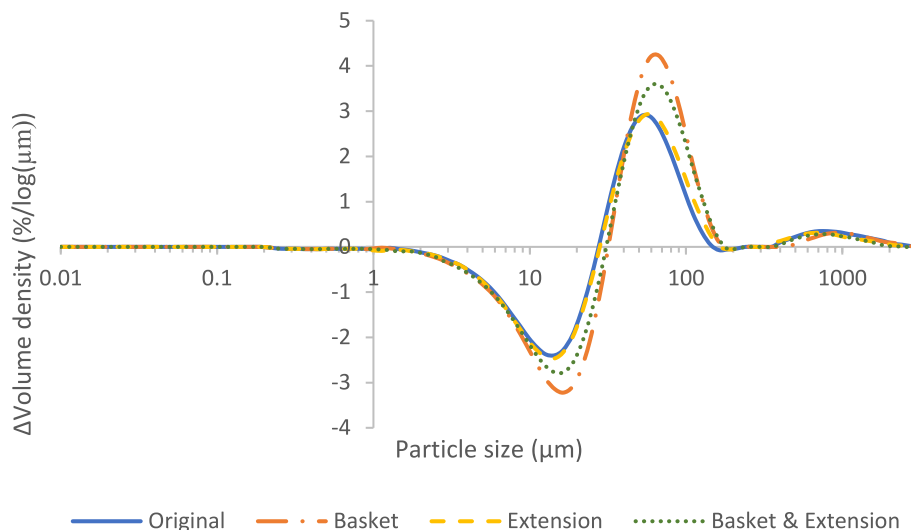


Fig. 9. Difference plots to evaluate particle size enlargement for different configurations with fines dosing.

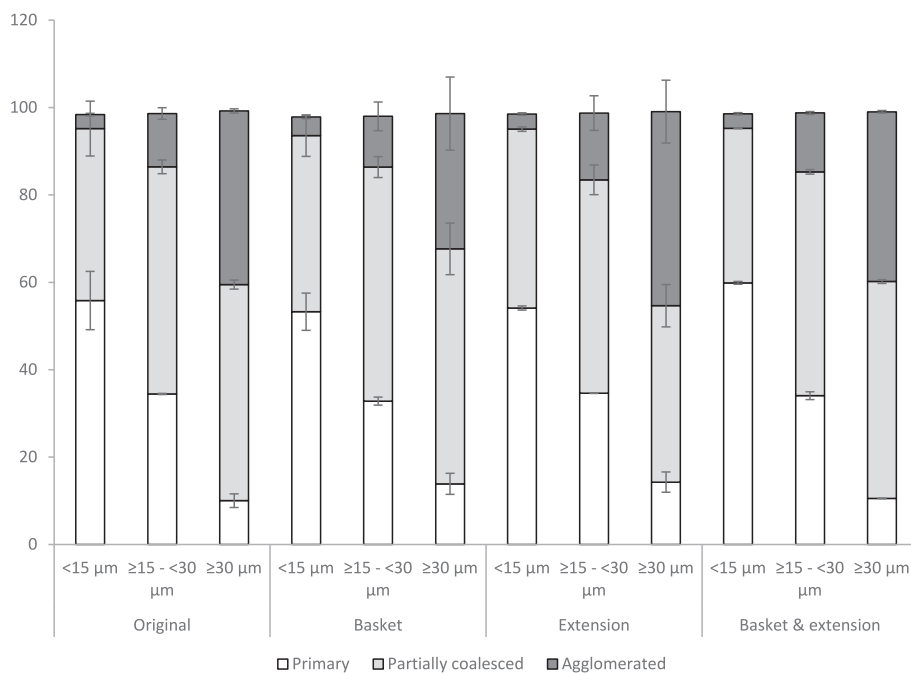


Fig. 10. Morphological classification of the powders produced in the different configurations, separated on size (based on the CE-diameter).

Table 3

Summed number of particle collision outcomes in the defined cylinder below the nozzle per time step of $1 \cdot 10^{-4}$ s (averaged for $n = 100$ times steps) for each configuration.

	Bounce	Coalescence	Coalescence as % of total collisions
A: Original	$1.16 \cdot 10^{10} \pm 5.4 \cdot 10^7$	$5.37 \cdot 10^8 \pm 4.8 \cdot 10^7$	4.4%
B: Basket	$8.71 \cdot 10^9 \pm 1.1 \cdot 10^8$	$5.31 \cdot 10^8 \pm 4.2 \cdot 10^7$	5.7%
C: Extension	$1.02 \cdot 10^{10} \pm 1.6 \cdot 10^9$	$3.82 \cdot 10^8 \pm 4.8 \cdot 10^7$	3.6%
D: Basket & extension	$1.59 \cdot 10^{10} \pm 1.4 \cdot 10^9$	$4.88 \cdot 10^8 \pm 1.0 \cdot 10^8$	3.0%

Table 4

Ranking agglomeration results of different configurations obtained by the different methods.

SEM	Indication of agglomeration (from left to right from indication of most agglomeration to least agglomeration)					
	D	>	B	>	A	≈ C
PSD	B	>	D	>	A	≈ C
$N_{PC} + N_{agg}$	B	≈	C	>	A	> D
Collisions CFD	A	>	B	>	D	> C

can serve as an explanation for the slightly larger quantity of particles <15 μm for configuration D (Appendix 1, Fig. A4). The particle morphology classification over the different size classes is similar to the other configurations (Fig. 10).

3.4.4. Collision outcomes

A successful collision in the CFD simulations is defined as a collision outcome of coalescence. In reality, there is a further distinction between coalescence, partial coalescence, and agglomeration, but to date, no such detailed collision maps exist. Slightly more collisions occurred with the higher nozzle position (configurations A and B) (Table 3). Since these results are not reflected in the experimental results, a question remains whether these collisions end up in the sample or as wall deposits in the spray dryer. Reducing the air swirl slightly lowers the fraction of successful collisions in both nozzle positions. The simulated collision outcomes are more in line with the morphology classification than with the difference plots. The basket & extension configuration (D) had the lowest amount of successful collisions in the simulations and the highest percentage of primary particles in the morphological classification. However, just as in the difference plots and in the morphological classification, the absolute differences are very small.

3.4.5. Combined agglomeration results

Overall, both the experimental results and the simulation results were inconclusive when it comes to agglomeration. The differences, if present, are small, and different methods do not necessarily lead to the same conclusions (Table 4). This provides some degrees of freedom when designing the air distribution for a spray dryer. However, it is still possible that small differences are amplified in a multi-stage spray dryer. Another option still is that agglomeration is more a fact of overlapping lances and their direction, the position of the fines return in relation to the spray, and drying conditions, rather than the air distribution. For example, when concerned with the drying conditions at a lower inlet air temperature might result in more agglomeration [8].

4. Conclusion

The impact of different configurations of an air distributor on the operability and nozzle zone agglomeration was investigated using CFD simulations and experiments at the pilot scale. Two levels of air swirl and two positions of nozzle and fines introduction were compared. The position of the nozzle and fines introduction greatly impacted the operability of the dryer. A high position close to the roof of the dryer (6 cm into drying chamber) resulted in a lot of fouling on the roof, which is usually undesired. Combining the high nozzle position with a lower level of air swirl reduced fouling on the roof but caused bearding on the nozzle. This configuration was therefore deemed inoperable. Lowering the position of the nozzle and fines introduction 25 cm further into the

drying chamber (in total 31 cm into the drying chamber) reduced fouling. This was therefore preferred over the higher position.

In terms of agglomeration, the results from both the experiments and the simulation were inconclusive. Air distribution seems to hardly affect agglomeration in such systems. Perhaps the minor effects can be amplified in spray dryers with fines recirculation.

The outcomes of this research can be used to design spray dryers. Our findings highlight the big effect of nozzle position on fouling. Reducing fouling enables longer consecutive operation of the dryer and less product that is wasted. We, therefore, advise spray dryer equipment manufacturers to perform an optimization study for their drying chamber and air distributor to find the ideal position. Regarding agglomeration, equipment manufacturers have some freedom in the design of the air distribution as this did not have a big impact. Other methods to stimulate agglomeration, for example using multiple lances with overlapping sprays, can be considered.

CRedit authorship contribution statement

Anneloes P. van Boven: Investigation, Conceptualization, Methodology, Writing – original draft. **Arend Dubbelboer:** Writing – original draft, Methodology, Investigation, Formal analysis. **Tom J.A. Janssen:** Writing – review & editing, Formal analysis. **Jewe Schröder:** Writing – review & editing, Funding acquisition, Conceptualization. **Jos J.W. Sewalt:** Resources, Writing – review & editing. **Reinhard Kohlus:** Conceptualization, Funding acquisition, Supervision, Writing – review & editing. **Maarten A.I. Schutyser:** Conceptualization, Funding acquisition, Supervision, Writing – review & editing.

Declaration of competing interest

This work is an Institute for Sustainable Process Technology (ISPT) project, i.e. StAggloP (Project number: DR-50-15). Partners in this project are Corbion, Danone, DSM-Firmenich, FrieslandCampina, University of Hohenheim, Wageningen University & Research, and ISPT. This project is co-funded with subsidy from the Topsector Energy by the Dutch Ministry of Economic Affairs and Climate Policy.

None of the authors has any conflict of interest to declare.

Data availability

Data will be made available on request.

Acknowledgments

This work is an Institute for Sustainable Process Technology (ISPT) project, i.e. StAggloP (Project number: DR-50-15). Partners in this project are Corbion, Danone, DSM-Firmenich, FrieslandCampina, University of Hohenheim, Wageningen University & Research, and ISPT. This project is co-funded with subsidy from the Topsector Energy by the Dutch Ministry of Economic Affairs and Climate Policy. We would like to thank David Hollestelle and André Sanders for their support in setting up the spray dryer configurations, Hans de Rooij for his assistance in creating the CAD of the spray dryer, Kyle van Schijndel for creating the perforated basket, Maurice Strubel for the SEM images, and Jord Dickhof, Luran Geertzen and Santiago Calderon Novoa for their assistance in the execution of the pre-trials.

Appendix 1



Fig. A1. Detailed picture from the perforated basket inserted in the air distributor.

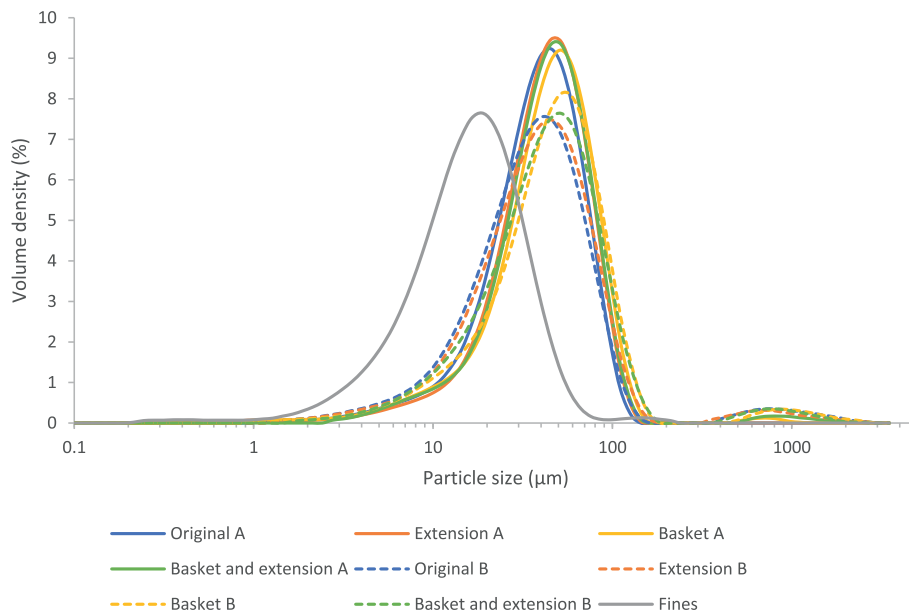


Fig. A2. Particle size distributions of the powdered samples. A are the powders without fines dosing, B are the powders during which fines were dosed.

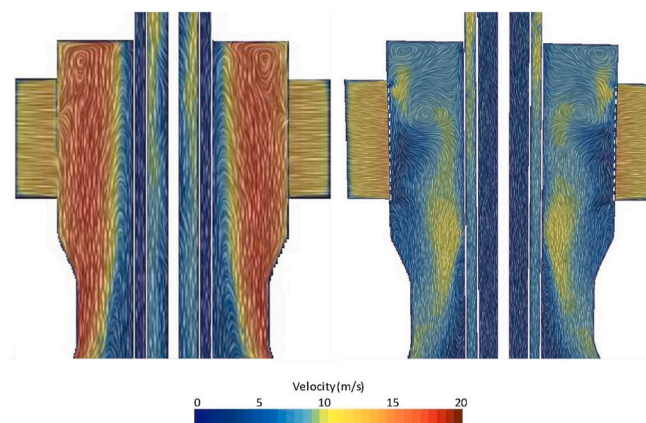


Fig. A3. Air velocity and direction in a cross-plane of the air distributor. Left: no perforated basket, right: with perforated basket.

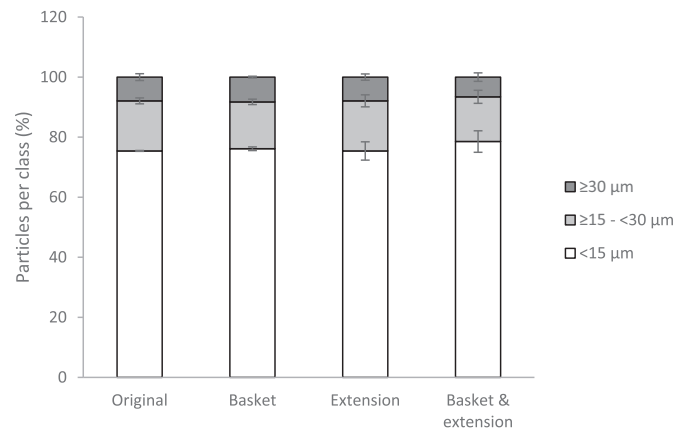


Fig. A4. Particle size classification based on CE-diameter.

Appendix 2: CFD model parameters

Mesh:

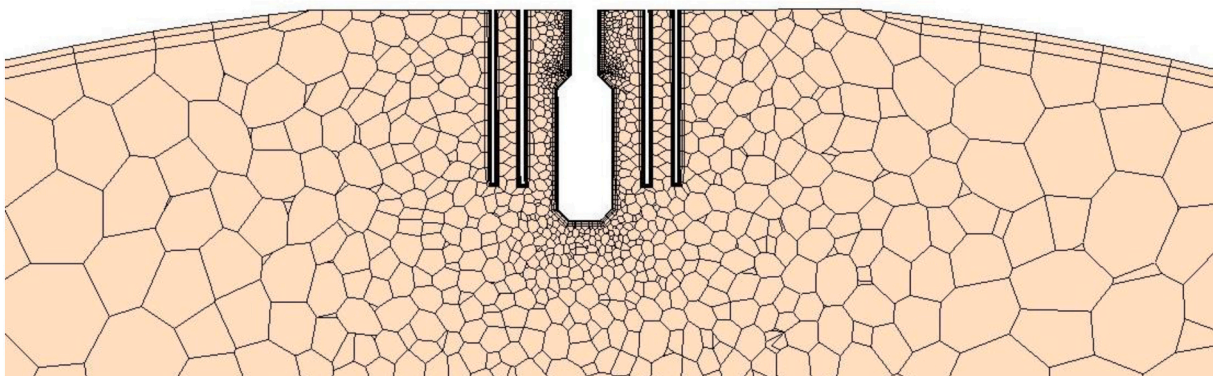
- Type: polyhedral
- Base size: 0.05 m
- Wall mesh: prism layer
- Prism layer near wall thickness: 4 mm
- All $y+$ wall treatment: wall $y+ > 30$

Mesh refinement around air lances, fines return transport air inlet, shielding air inlet and main air inlet.

- Base size: 0.0125 m
- Prism values:
 - o 4 layers
 - o Prism layer near wall thickness: 0.4 mm giving max wall $y+ = 3.0$
 - o Total prism layer thickness: 0.0035 mm

Resulting mesh metrics from the spray dryer with basket (considered the most difficult mesh):

- Maximum skewness angle: 82.8 degrees
- Face validity 100% > 1.0 (cells with a face validity below 1.0 are considered bad)
- Minimum volume change: 0.01 (cells with a volume change of 0.01 or lower are considered bad cells)
- Maximum volume change: 1.0
- Cell aspect ratio: 0.185–1.0



Solver: segregated flow, species and energy

- Implicit unsteady
- Time step: 1-E-4 s resulting max convective Courant number: 1.85

- Temporal discretization: 1st order
- Inner iterations: 5

Lagrangian solver:

- Maximum courant number: 0.7
- Minimum courant number: 0.15
- Parcel streams: 250
- 2nd order Tracking Integration Method

Lewis number (Le) = 1.0.

Turbulent Prandtl number = 0.9.

Turbulent Schmidt number = 0.9.

Collision model details.

The collision efficiency E_i is calculated by:

$$E_i = \min \left[1.0, A \left(\frac{We - We_c}{g(\gamma)} \right)^a \right]$$

where $g(\gamma) = a_3 \cdot \gamma^3 + a_2 \cdot \gamma^2 + a_1 \cdot \gamma + a_0$, and $\gamma = \frac{r_2}{r_1}$ with $r_2 > r_1$.

$a_0 = 0.434$.

$a_1 = 29.767$.

$a_2 = 9.187$.

$a_3 = 4.651$.

Parameter	B_{coal}	B_{bounce}
a	-0.485	0.163
A	0.085	0.693
We_c	-9.999E-05	2.5

We = the collision weber number $We_{\text{coll}} = \frac{\rho_l (v_{1,2})^2 (r_1 + r_2)}{2\sigma}$

We_c = empirical constant

r_1 and r_2 are the particle radii of the colliding particles

σ = the surface tension

ρ_l = density of the air

$v_{1,2}$ = velocity difference of the colliding particles.

References

- [1] L. Ozmen, T.A.G. Langrish, An experimental investigation of the wall deposition of milk powder in a pilot-scale spray dryer, *Dry. Technol.* 21 (2003) 1253–1272, <https://doi.org/10.1081/DRT-120023179>.
- [2] K. Samborska, S. Poozesh, A. Barańska, M. Sobulska, A. Jedlińska, C. Arpagaus, N. Malekjani, S.M. Jafari, Innovations in spray drying process for food and pharma industries, *J. Food Eng.* 321 (2022), <https://doi.org/10.1016/j.jfoodeng.2022.110960>.
- [3] C. Turchiuli, A. Gianfrancesco, S. Palzer, E. Dumoulin, Evolution of particle properties during spray drying in relation with stickiness and agglomeration control, *Powder Technol.* 208 (2011) 433–440, <https://doi.org/10.1016/j.powtec.2010.08.040>.
- [4] I. Filková, L.X. Huang, A.S. Mujumdar, *Handbook of Industrial Drying - Chapter 9: Industrial Spray Drying Systems*, 3rd ed., CRC Press, 2007.
- [5] L. Huang, K. Kumar, A.S. Mujumdar, Use of computational fluid dynamics to evaluate alternative spray dryer chamber configurations, *Dry. Technol.* 21 (2003) 385–412, <https://doi.org/10.1081/DRT-120018454>.
- [6] R.E.M. Verdurmen, M. Verschuere, M. Gusing, H. Straatsma, S. Blei, M. Sommerfeld, Simulation of agglomeration in spray dryers: the EDECAD project, *Lait* 85 (2005) 343–351, <https://doi.org/10.1051/lait:2005023>.
- [7] N.M. Eijkelboom, A.P. van Boven, I. Siemons, P.F.C. Wilms, R.M. Boom, R. Kohlus, M.A.I. Schutyser, Particle structure development during spray drying from a single droplet to pilot-scale perspective, *J. Food Eng.* 337 (2023) 111222, <https://doi.org/10.1016/j.jfoodeng.2022.111222>.
- [8] A.P. van Boven, S.M. Calderon Novoa, R. Kohlus, M.A.I. Schutyser, Investigation on nozzle zone agglomeration during spray drying using response surface methodology, *Powder Technol.* 429 (2023) 118910, <https://doi.org/10.1016/j.powtec.2023.118910>.
- [9] R. Kuriakose, C. Anandharamkrishnan, *Computational Fluid Dynamics (CFD) Applications in Spray Drying of Food Products*, 2024, <https://doi.org/10.1016/j.tifs.2010.04.009>.
- [10] N.A. Ruprecht, R. Kohlus, Determination and modelling of the particle size dependent residence time distribution in a pilot plant spray dryer, in: *Universitat Politècnica de Valencia*, 2019, <https://doi.org/10.4995/ids2018.2018.7740>.
- [11] N. Ruprecht, J. Senge, H. Teichmann, R. Kohlus, Modelling and Measurement of the Particle Size Dependent Residence Time Distribution in Spray Drying, 2019.
- [12] A. Gianfrancesco, C. Turchiuli, D. Flick, E. Dumoulin, CFD modeling and simulation of maltodextrin solutions spray drying to control stickiness, *Food Bioprocess Technol.* 3 (2010) 946–955, <https://doi.org/10.1007/s11947-010-0352-2>.
- [13] A.M. Goula, K.G. Adamopoulos, Influence of spray drying conditions on residue accumulation - simulation using CFD, *Dry. Technol.* 22 (2004) 1107–1128, <https://doi.org/10.1081/DRT-120038583>.
- [14] T. Ullum, J. Sloth, A. Brask, M. Wahlberg, Predicting spray dryer deposits by CFD and an empirical drying model, *Dry. Technol.* 28 (2010) 723–729.
- [15] H. Jubaer, J. Xiao, X.D. Chen, C. Selomulya, M.W. Woo, Identification of regions in a spray dryer susceptible to forced agglomeration by CFD simulations, *Powder Technol.* 346 (2019) 23–37, <https://doi.org/10.1016/j.powtec.2019.01.088>.
- [16] F. Hussain, M. Jaskulski, M. Piatkowski, E. Tsotsas, CFD simulation of agglomeration and coalescence in spray dryer, *Chem. Eng. Sci.* 247 (2022), <https://doi.org/10.1016/j.ces.2021.117064>.
- [17] R.E.M. Verdurmen, G. Van Houwelingen, M. Gusing, M. Verschuere, J. Straatsma, Agglomeration in spray drying installations (the EDECAD project): stickiness measurements and simulation results, *Dry. Technol.* 24 (2006) 721–726, <https://doi.org/10.1080/07373930600684973>.
- [18] G. Finotello, R.F. Kooiman, J.T. Padding, K.A. Buist, A. Jongasma, F. Innings, J.A. M. Kuipers, The dynamics of milk droplet–droplet collisions, *Exp. Fluids* 59 (2018) 1–19, <https://doi.org/10.1007/s00348-017-2471-2>.
- [19] A.M. Williams, *Instant Milk Powder Production: Determining the Extent of Agglomeration*, PhD, Massey University, Palmerston North, 2007.
- [20] *Siemens Digital Industries Software, Simcenter STAR-CCM+, 2024*.
- [21] *Siemens Digital Industries Software, Simcenter STAR-CCM+ User Guide, Elliptic Blending Model*. <https://docs.sw.siemens.com/documentation/ext>

- ernal/PL20200805113346338/en-US/userManual/userguide/html/index.html#page/STARCCMP%2FGUID-D41C365F-94BA-4086-B9F6-629F8A6427DD.html, 2024 (accessed January 24, 2024).
- [22] Siemens Digital Industries Software, Simcenter STAR-CCM+ User Guide, Primary Atomization. <https://docs.sw.siemens.com/documentation/external/PL20200805113346338/en-US/userManual/userguide/html/index.html#page/STARCCMP%2FGUID-7DB3DC43-B7E7-43A8-8645-97333CD343AE.html%23wwID0EFFIMD>, 2024 (accessed January 24, 2024).
- [23] S.N. Saleh, CFD simulations of a co-current spray dryer, *Int. J. Chem. Molec. Eng.* 4 (2010) 226–231.
- [24] Siemens Digital Industries Software, Simcenter STAR-CCM+ User Guide, NTC Collision Model Reference. <https://docs.sw.siemens.com/documentation/external/PL20200805113346338/en-US/userManual/userguide/html/index.html#page/STARCCMP%2FGUID-FE90C25A-5D5E-4BC8-A585-0F042B2570E9.html>, 2024 (accessed January 25, 2024).
- [25] H. Jubaer, S. Afshar, G. Le Maout, S. Mejean, C. Selomulya, J. Xiao, X.D. Chen, R. Jeantet, M.W. Woo, The impact of self-sustained oscillations on particle residence time in a commercial scale spray dryer, *Powder Technol.* 360 (2020) 1177–1191, <https://doi.org/10.1016/j.powtec.2019.11.023>.
- [26] T.A.G. Langrish, I. Zbicinski, The effects of air inlet geometry and spray cone angle on the wall deposition rate in spray dryers, *Trans. Inst. Chem. Eng.* 72 (1994) 420–430.
- [27] M. Djaeni, S.B. Sasongko, A.J.B. Van Boxtel, Enhancement of Energy Efficiency and Food Product Quality Using Adsorption Dryer with Zeolite Article History. www.ijred.com, 2013.
- [28] M.G. Bordón, N.P.X. Alasino, Á. Villanueva-Lazo, C. Carrera-Sánchez, J. Pedroche-Jiménez, M.C. del Millán-Linares, P.D. Ribotta, M.L. Martínez, Scale-up and optimization of the spray drying conditions for the development of functional microparticles based on chia oil, *Food Bioprod. Process.* 130 (2021) 48–67, <https://doi.org/10.1016/j.fbp.2021.08.006>.
- [29] M. Aghbashlo, H. Mobli, S. Rafiee, A. Madadlou, Energy and exergy analyses of the spray drying process of fish oil microencapsulation, *Biosyst. Eng.* 111 (2012) 229–241, <https://doi.org/10.1016/j.biosystemseng.2011.12.001>.
- [30] J.A. Fröhlich, M. Spiess, J. Hinrichs, R. Kohlus, Nozzle zone agglomeration in spray dryers: process dependency of the fines mass flow and its importance for agglomerate formation, *Dry. Technol.* (2022) 1–13, <https://doi.org/10.1080/07373937.2022.2111439>.
- [31] J. Pisecky, Handbook of Milk Powder Manufacture, Second, GEA Process Engineering A/S, Copenhagen, 2012. www.niro.com.